

Rogue waves, rational solitons, and modulational instability in an integrable fifth-order nonlinear Schrödinger equation

Yunqing Yang^{1,2}, Zhenya Yan^{3,*} and Boris A. Malomed⁴

¹*School of Mathematics, Physics and Information Science, Zhejiang Ocean University, Zhoushan, Zhejiang 316022, China*
²*Key Laboratory of Oceanographic Big Data Mining & Application of Zhejiang Province, Zhoushan, Zhejiang 316022, China*

³*Key Laboratory of Mathematics Mechanization, Institute of Systems Science, AMSS, Chinese Academy of Sciences, Beijing 100190, China*

⁴*Department of Physical Electronics, School of Electrical Engineering, Tel Aviv University, Tel Aviv 59978, Israel*

We analytically study rogue-wave (RW) solutions and rational solitons of an integrable fifth-order nonlinear Schrödinger (FONLS) equation with three free parameters. It includes, as particular cases, the usual NLS, Hirota, and Lakshmanan-Porsezian-Daniel (LPD) equations. We present continuous-wave (CW) solutions and conditions for their modulation instability in the framework of this model. Applying the Darboux transformation to the CW input, novel first- and second-order RW solutions of the FONLS equation are analytically found. In particular, trajectories of motion of peaks and depressions of profiles of the first- and second-order RWs are produced by means of analytical and numerical methods. The solutions also include newly found rational and W-shaped one- and two-soliton modes. The results predict the corresponding dynamical phenomena in extended models of nonlinear fiber optics and other physically relevant integrable systems.

Solitons are usually generated by the balance of linear dispersion and nonlinear self-focusing. Rogue waves (RWs), as a special type of solitary waves, are driven by a similar mechanism acting on top of a modulationally unstable flat background (alias continuous wave, CW). In particular, the celebrated nonlinear Schrödinger (NLS) equation with the self-focusing sign of the nonlinearity gives rise to both bright solitons and RWs, which are used to model nonlinear phenomena in diverse fields, such as nonlinear optics, deep ocean, plasmas, Bose-Einstein condensates, and biophysics. In nonlinear fiber optics, the correct description of tall narrow pulses produced by the RWs makes necessary to include higher-order effects, such as the stimulated Raman scattering, nonlinear group-velocity dispersion (alias the shock term), and third-order dispersion. In the general case, the addition of such terms to the NLS equation breaks its integrability, making it impossible to find solitons and RWs in an analytical form. However, under special conditions the respective extended NLS equation may keep the integrability. In particular, quite a general model of the latter type, namely, the fifth-order NLS (FONLS) equation, which includes three free parameters, was recently found. Its particular forms amount to other previously known integrable equations, such as the usual NLS, Hirota, and Lakshmanan-Porsezian-Daniel (LPD) equations. In this paper, our objective is

to use the integrability of the FONLS equation for constructing its exact RW solutions. Because RWs are driven by the modulational instability of flat CW states, we first present the CW solutions of this model and conditions for their modulation instability. Then we proceed to the core part of the analysis, which reveals novel exact first- and second-order RW solutions, by means of the Darboux transformation applied to the CW input. The solutions are obtained in the form of explicit rational functions of the spatial coordinate and time. In particular, interesting results are produced by the analysis of trajectories of the motion of peaks and depressions of the RW profiles. Furthermore, the obtained rational solutions include new W-shaped one- and two-soliton modes of the FONLS equation. The analysis developed in this work and results produced by it may suggest new possibilities to analyze other sophisticated nonlinear models of practical significance.

I. INTRODUCTION

Rogue waves (RWs, also known as monster waves, killer waves, giant waves, extreme waves, etc.) [1, 2], as a kind of localized modes, are generated, in the paradigmatic form [3], by the self-focusing nonlinear Schrödinger (NLS) equation for wave amplitude $\psi(x, t)$,

$$i\psi_x + \frac{1}{2}\psi_{tt} + |\psi|^2\psi = 0. \quad (1)$$

as a limit case of the Ma-breather [4] or Akhmediev-breather [5] solutions on top of a flat continuous-wave

* zyyan@mmlrc.iss.ac.cn

(CW) state, which is subject to the modulational instability (MI) [5]. This equation is written in terms of the guided-wave notation, with x and t being the propagation distance and reduced time, respectively [6, 7]. The RWs are sometimes called *rogons*, if they reappear unaffected in the size and shape after their interactions [8].

The RW phenomenon was initially found in the deep ocean [1, 2]. Recently, it has also drawn growing interest in other fields, such as Bose-Einstein condensates (BEC), nonlinear optics, plasma physics, and even dynamics of financial markets [9–15]. Generally speaking, the RWs are spatially and temporally localized excitations which seem “to appear from nowhere and disappear without a trace” [16], that makes it difficult to systematically observe them in the ocean, where they had been originally spotted. The origin of the RWs is still a subject of discussions [17], stimulating the development of various theoretical approaches and laboratory experiments [18, 19]. In particular, it is well established that the MI of the CW background, also known as the Benjamin-Feir instability [20], plays a pivotal role in the generation of RWs [21–24].

In addition to the basic RW solutions of the NLS equation, RWs have been found in related integrable equations including higher-order dispersion and nonlinearity terms, such as Hirota [25], Sasa-Satsuma [26, 27], Gerdjikov-Ivanov [28, 31], Lakshmanan-Porsezian-Daniel (LPD) [29], quintic NLS [30], modified NLS [31], and Davey-Stewartson [32] equations, the derivative NLS equations of the Chen-Lee-Liu and Kaup-Newell types [33], coupled NLS equations [35, 36], three-wave equations [37], and various modifications of these models with variable coefficient [38–40]. Finding RWs and rational solitons of other nonlinear wave equations in the field of nonlinear science remains a relevant subject.

Recently, Chowdury *et al.* [41] reported an integrable three-parameter fifth-order NLS (FONLS) equation, written as

$$i\psi_x + S(\psi) - i\alpha H(\psi) + \gamma P(\psi) - i\delta Q(\psi) = 0, \quad (2)$$

where $\psi \equiv \psi(x, t)$ is a complex field, subscripts denote partial derivatives with respect to the corresponding variables, while α , γ , and δ are all real parameters. Further, $S(\psi)$ denotes the NLS part

$$S(\psi) = \frac{1}{2}\psi_{tt} + |\psi|^2\psi,$$

$H(\psi)$ stands for the Hirota part,

$$H(\psi) = \psi_{ttt} + 6|\psi|^2\psi_t,$$

$P(\psi)$ is the LPD part,

$$P(\psi) = \psi_{ttt} + 8|\psi|^2\psi_{tt} + 6|\psi|^4\psi + 4|\psi_t|^2\psi + 6\psi^*\psi_t^2 + 2\psi^2\psi_{tt}^*,$$

and $Q(\psi)$ is the quintic part,

$$Q(\psi) = \psi_{ttttt} + 10|\psi|^2\psi_{ttt} + 10\left(\psi|\psi_t|^2\right)_t + 20\psi^*\psi_t\psi_{tt} + 30|\psi|^4\psi_t,$$

where ψ^* stands for the complex conjugate of ψ . This equation (2) is a member of the NLS hierarchy introduced by Kano [42] and contains many special cases. When $\alpha = \gamma = \delta = 0$, Eq. (2) reduces to the fundamental NLS equation (1). As $\gamma = \delta = 0$, it becomes the Hirota equation [43]. When $\alpha = \delta = 0$, it is the LPD equation [44]. All these particular nonlinear wave equations are integrable, and the respective soliton solutions have been obtained using different methods. Equation (2) with $\alpha = \gamma = 0$ is also integrable, and its soliton and breather solutions are available too [30, 41].

To the best of our knowledge, rational RW solutions of Eq. (2) with arbitrary parameters (α , γ , and δ) have not been reported before. In this work, we aim to produce such localized solutions and study their dynamical properties by means of the generalized Darboux transform.

The rest of the paper is organized as follows. In Sec. II, the Lax pair and Darboux transform with nonzero CW background are introduced for Eq. (2). In Sec. III, the MI of the CW states is investigated, as the driving mechanism behind the existence of RWs. In Sec. IV, the first- and second-order RW solutions for Eq. (2) are explicitly found by means of the Darboux transform applied to the flat CW. Trajectories of motion of peaks and depressions of the derived RWs are explicitly considered, to demonstrate the structure and dynamics of these patterns. Rational W-shaped solitons of the FONLS equation, which differ from the usual bright and dark solitons, are also found for special parameter values. The paper is concluded by Sec. V.

II. THE LAX PAIR, DARBOUX TRANSFORM, AND CW SOLUTIONS

Equation (2) is integrable in terms of the corresponding Lax pair, which can be obtained as the compatibility condition, $R_{xt} = R_{tx}$, i.e., $U_x - V_t + [U, V] = 0$, for the following linear spectral problem [41]:

$$R_t = UR, \quad U = \lambda J + U_0, \quad (3)$$

$$R_x = VR, \quad V = \lambda U + V_0 + \alpha L + \gamma M + \delta N, \quad (4)$$

where λ is a complex spectral parameter, the Jost function $R \equiv R(x, t)$ is a column vector given by

$$R = R(x, t) = \begin{pmatrix} r \\ s \end{pmatrix}, \quad (5)$$

with $r = r(x, t)$ and $s = s(x, t)$ being complex functions, and matrices J, U_0, V_0, L, M, N given by

$$\begin{aligned} J &= \begin{bmatrix} i & 0 \\ 0 & -i \end{bmatrix}, \\ U_0 &= \begin{bmatrix} 0 & i\psi^* \\ i\psi & 0 \end{bmatrix}, \\ V_0 &= \frac{1}{2} \begin{bmatrix} -i|\psi|^2 & \psi_t^* \\ -\psi_t & i|\psi|^2 \end{bmatrix}, \\ L &= -4(\lambda^3 J + \lambda^2 U_0 + \lambda V_0) + L_0, \\ M &= 2\lambda L + M_0, \\ N &= -2\lambda M + N_0, \end{aligned} \quad (6)$$

where

$$\begin{aligned} L_0 &= \begin{bmatrix} \psi\psi_t^* - \psi^*\psi_t & i(2|\psi|^2\psi^* + \psi_{tt}^*) \\ i(2|\psi|^2\psi + \psi_{tt}) & \psi^*\psi_t - \psi\psi_t^* \end{bmatrix}, \\ M_0 &= \begin{bmatrix} m_1 & m_2 \\ m_3 & -m_1 \end{bmatrix}, \\ N_0 &= \begin{bmatrix} n_1 & n_2 \\ n_3 & -n_1 \end{bmatrix}, \\ m_1 &= -i(3|\psi|^4 + \psi\psi_{tt}^* - \psi_t\psi_t^* + \psi^*\psi_{tt}), \\ m_2 &= -m_3^* \\ &= 6|\psi|^2\psi_t^* + \psi_{ttt}^*, \\ n_1 &= (\psi - \psi^*)\psi_{ttt} - \psi_t\psi_{tt}^* + \psi_t^*\psi_{tt} \\ &\quad + 6|\psi|^2(\psi\psi_t^* - \psi^*\psi_t), \\ n_2 &= -n_3^* \\ &= 6i|\psi|^4\psi^* + 2i\psi^{*2}\psi_{tt} + 4i|\psi_t|^2\psi^* + 6i\psi\psi_t^{*2} \\ &\quad + 8i|\psi|^2\psi_{tt}^* + i\psi_{ttt}^*. \end{aligned} \quad (7)$$

Based on the Lax pair of an integrable nonlinear wave equation, the Darboux transform is a powerful method for generating soliton and breather solutions, using a zero solution or a flat CW as the ‘‘seed’’ solution [48]. The hierarchy of multisoliton states [45] can be derived starting from zero, while solutions related to the MI [46] are obtained starting from the CW.

The Darboux transform for Eq. (2) is given by

$$\psi_{n+1}(x, t) = \psi_n(x, t) - \frac{4is_{n+1}(x, t)r_{n+1}^*(x, t)}{|r_{n+1}(x, t)|^2 + |s_{n+1}(x, t)|^2}, \quad (8)$$

where $n = 0, 1, 2, \dots$, $\psi_n(x, t)$ is a seed solution of Eq. (2), while $\psi_{n+1}(x, t)$ is a new solution generated from $\psi_n(x, t)$, while $r_{n+1}(x, t)$ and $s_{n+1}(x, t)$ are solutions of the linear spectral problem based on Eqs. (3)-(7), with $\psi(x, t)$ substituted by $\psi_{n+1}(x, t)$. We here choose $\lambda = i$ in system (3)-(7), as this value of the spectral parameter corresponds to RW solutions of Eq. (2).

The zero seed solution was employed to build multi-soliton solutions of Eq. (2) in Ref. [41]. In order to use

the Darboux transform (8) for obtaining RW solutions of Eq. (2), we here take the CW solution of Eq. (2),

$$\psi_0(x, t) = ae^{i(bx+ct)}, \quad (9)$$

as the seed, where $a \neq 0$ and c are arbitrary real constants, and

$$\begin{aligned} b &= \alpha c(6a^2 - c^2) + \gamma(6a^4 - 12a^2c^2 + c^4) \\ &\quad + c\delta(30a^4 - 20a^2c^2 + c^4) - \frac{c^2}{2} + a^2. \end{aligned} \quad (10)$$

Lastly, we note that FONLS equation (2) is invariant under the following scale transformation:

$$\begin{aligned} x &\rightarrow \mu^2 x, \quad t \rightarrow \mu t, \quad \psi \rightarrow \frac{\psi}{\mu}, \\ \alpha &\rightarrow \mu\alpha, \quad \gamma \rightarrow \mu^2\gamma, \quad \delta \rightarrow \mu^3\delta, \end{aligned}$$

where μ is an arbitrary real constant. We stress that this invariance is different from that for the NLS equation [34].

III. THE MODULATIONAL INSTABILITY (MI) OF CW STATES

To investigate the MI of the CW solution (9), subject to constraint (10), we add perturbations $\phi(x, t)$ with an infinitesimal amplitude ε ,

$$\hat{\psi}(x, t) = [a + \varepsilon\phi(x, t)]e^{i(bx+ct)}, \quad (11)$$

which is followed by the derivation of the linearized equation for the perturbation:

$$\begin{aligned} i\phi_x - i\delta\phi_{tttt} + (\gamma + 5c\delta)\phi_{ttt} + i(10c^2 - 10a^2\delta \\ + 4c\gamma - \alpha)\phi_{ttt} + (40a^2c\delta + 3c\alpha - 6c^2\gamma - 10c^3\delta \\ + 8a^2\gamma + 1/2)\phi_{tt} + 2a^2(5c\delta + \gamma)\phi_{tt}^* + i(-30a^4 \\ + 60a^2c^2\delta - 5c^4\delta + 24a^2c\gamma - 4c^3\gamma - 6a^2\alpha \\ + 3c^2\alpha + c)\phi_t + a^2(60a^2c\delta - 20c^3\delta + 12a^2\gamma \\ - 12c^2\gamma + 6c\alpha + 1)(\phi + \phi^*) = 0. \end{aligned} \quad (12)$$

Relevant solutions to Eq. (12) with wavenumber k and frequency ω are sought for as

$$\phi(x, t) = F \cos(kx - \omega t) + iG \sin(kx - \omega t), \quad (13)$$

where F and G are real amplitudes. The substitution of ansatz (13) into Eq. (12) readily leads to the following dispersion relation for the perturbations, obtained as the condition for the existence of nontrivial solutions for F

and G :

$$\begin{aligned}
& 4 \{ k - \omega [c + \alpha(3c^2 - 6a^2 + k^2) + 4\gamma c(6a^2 - c^2 - k^2) \\
& + 5\delta(12a^2c^2 - 6a^4 + 2a^2k^2 - 2c^2\omega^2 - c^4 - \omega^4)] \}^2 \\
& = -\omega^2(4a^2 - \omega^2) [10c\delta(6a^2 - 2c^2 - \omega^2) \\
& + 2\gamma(6a^2 - 6c^2 - \omega^2) + 6\alpha c + 1]^2.
\end{aligned} \tag{14}$$

It follows from Eq. (14) that we know the wavenumber k is complex for frequencies interval

$$|\omega| < 2|a|,$$

hence the CW states are subject to the MI, and RW patterns may be expected as solutions of Eq. (2) in this case.

IV. ROGUE WAVES, RATIONAL SOLITONS, AND THE DYNAMICAL ANALYSIS

A. First-order rational solutions and trajectories of extreme points

We choose $a = 1$ and $c = 0$ in the seed solution given by Eqs. (9) and (10), i.e.,

$$\psi_0(x, t) = e^{i(6\gamma+1)x}, \tag{15}$$

Solving the linear spectral problem (3)-(7) with $\lambda = i$ and the seed solution (15) yields eigenfunctions

$$\begin{aligned}
r_1(x, t) &= -c_0[2(t + vx + iBx) - 1]e^{-i(B+1)x/4}, \\
s_1(x, t) &= c_0[2(t + vx + iBx) + 1]e^{i(B+1)x/4},
\end{aligned} \tag{16}$$

where c_0 is an arbitrary nonzero constant, and v, B are given by

$$B = 12\gamma + 1, \quad v = 6(\alpha + 5\delta). \tag{17}$$

Then, substituting solution (15) and eigenfunctions (16) into the Darboux transform (8), we obtain the first-order rational solution of Eq. (2) as

$$\psi_1(x, t) = \left[1 - \frac{4(1 + 2iBx)}{D_1(x, t)} \right] \exp\left(\frac{i}{2}(B+1)x\right), \tag{18}$$

where we define

$$D_1(x, t) = 4(t + vx)^2 + 4B^2x^2 + 1, \tag{19}$$

From the first-order rational solution (18) of Eq. (2), the corresponding first-order RW solutions can be obtained also for the Hirota, LPD, and quintic NLS equations, by choosing the respective values of α, γ , and δ , as specified in Introduction. For example, for (i)

$\alpha = \delta = \gamma = 0$, we also find the known first-order RW solution of the self-focusing NLS equation,

$$\psi_{1,\text{NLS}} = \left[1 - \frac{4(1 + 2ix)}{4(t^2 + x^2) + 1} \right] e^{ix};$$

(ii) for $\delta = \gamma = 0$, we obtain the first-order RW solution of the Hirota equation,

$$\psi_{1,\text{Hirota}} = \left[1 - \frac{4(1 + 2ix)}{4(t + 6\alpha x)^2 + 4x^2 + 1} \right] e^{ix};$$

(iii) for $\alpha = \delta = 0$, the first-order RW solution of the LPD equation is obtained:

$$\psi_{1,\text{LPD}} = \left\{ 1 - \frac{4[1 + 2i(12\gamma + 1)x]}{4t^2 + 4(12\gamma + 1)^2x^2 + 1} \right\} e^{i(6\gamma+1)x}.$$

In the following we will analyze the solution (18) for two different cases $\gamma \neq -1/12$ and $\gamma = -1/12$, which display the distinguish profiles of solution (18).

1. The first-order RW solution with $\gamma \neq -1/12$

With $\gamma \neq -1/12$, the rational solution (18) of Eq. (2) is just its the first-order RW solution. To analyze dynamical properties of the RW solution, we consider its intensity,

$$|\psi_1(x, t)|^2 = \frac{8 - 32(t + vx)^2 + 32B^2x^2}{[1 + 4(t + vx)^2 + 4B^2x^2]^2} + 1. \tag{20}$$

It is easy to see that expression (20) has three critical points,

$$(x_1, t_1) = (0, 0), \quad (x_{2,3}, t_{2,3}) = \left(0, \pm \frac{\sqrt{3}}{2} \right),$$

which are three real roots of system $\{\partial(|\psi_1(x, t)|^2)/\partial t = 0, \partial(|\psi_1(x, t)|^2)/\partial x = 0\}$ (see Appendix A). Further, the critical point (x_1, t_1) is a maximum (peak), as

$$\frac{\partial^2(|\psi_1(x, t)|^2)}{\partial t^2} = -192 < 0,$$

and

$$\begin{aligned}
& \left(\frac{\partial^2(|\psi_1(x, t)|^2)}{\partial x \partial t} \right)^2 - \frac{\partial^2(|\psi_1(x, t)|^2)}{\partial t^2} \frac{\partial^2(|\psi_1(x, t)|^2)}{\partial x^2} \\
& = -12288(12\gamma + 1)^2 < 0
\end{aligned} \tag{21}$$

at point (x_1, t_1) , which makes the meaning of condition $\gamma \neq -1/12$ obvious. Similarly, two critical points $(x_{2,3}, t_{2,3})$ are minima (depressions), as

$$\frac{\partial^2(|\psi_1(x, t)|^2)}{\partial t^2} = 6 > 0,$$

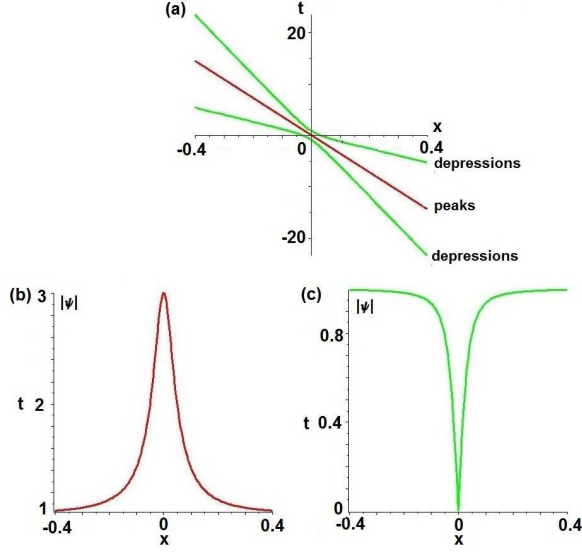


FIG. 1. (Color online). The first-order rogue wave (18) for $\alpha = \gamma = \delta = 1$: (a) The motion of the peak and depression centers. (b) The evolution of the peak absolute value. (c) The evolution of the absolute value of the field at the depression points.

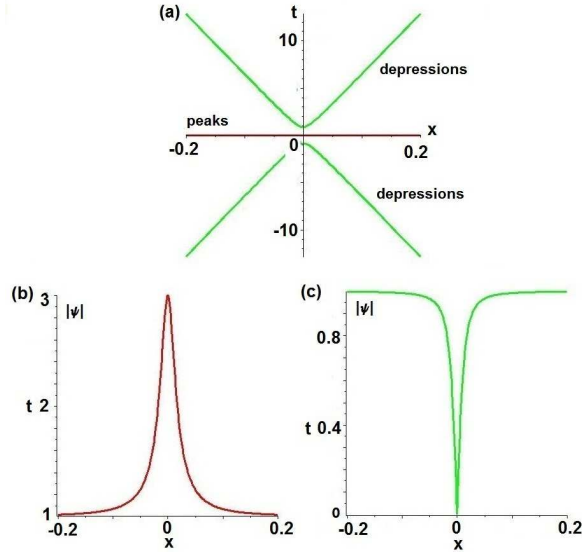


FIG. 2. (Color online). The same as in Fig. 1, but for parameters $\alpha = -5$, $\gamma = 3$, and $\delta = 1$.

and

$$\left(\frac{\partial^2 (|\psi_1(x,t)|^2)}{\partial x \partial t} \right)^2 - \frac{\partial^2 (|\psi_1(x,t)|^2)}{\partial t^2} \frac{\partial^2 (|\psi_1(x,t)|^2)}{\partial x^2} = -48(12\gamma + 1)^2 < 0 \quad (22)$$

at points $(x_{2,3}, t_{2,3})$.

Note that these critical points, (x_j, t_j) , $j = 1, 2, 3$, do not depend on parameters α , γ , and δ .

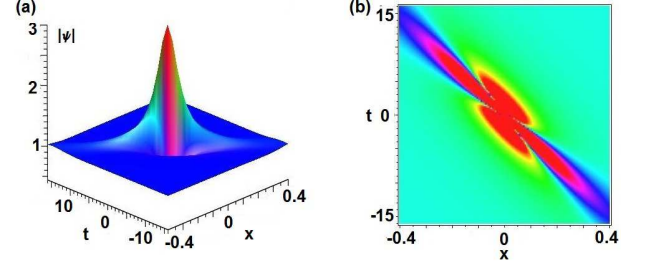


FIG. 3. (Color online). (a) The density evolution and (b) 2D density contour plots for the first-order RW solution (18) at $\alpha = \gamma = \delta = 1$. The corresponding motion of peaks and depressions is displayed in Fig. 1.

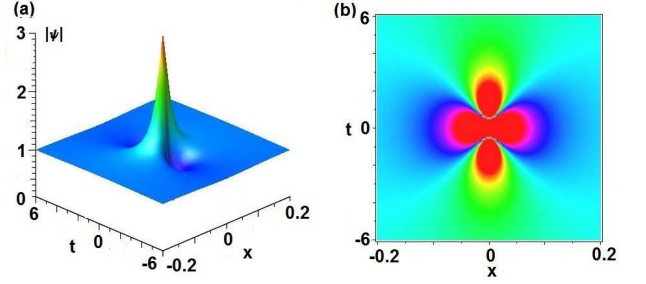


FIG. 4. (Color online). (a) The density evolution and (b) 2D density contour plots for the first-order RW solution (18) at $\alpha = -5$, $\gamma = 3$ and $\delta = 1$. The corresponding motion of peaks and depressions is displayed in Fig. 2.

The evolution of the first-order RW solution can be characterized by trajectories of peaks and depressions [47]. The trajectory of the peak's center is given by the dependence of its temporal coordinate, T_h , on x . It follows from Eq. (18) that

$$T_h = -vx, \quad (23)$$

and the temporal coordinates, $T_{c\pm}$, of centers of the two depressions are given by

$$T_{c\pm} = -vx \pm \frac{1}{2} \sqrt{3(1 + 4B^2x^2)}. \quad (24)$$

Thus, the motion of the peak is totally determined by parameter $v = 6(\alpha + 5\delta)$ defined in Eq. (17), while the RW width, which is defined as the temporal distance between the two depressions, i.e.,

$$T_d = \sqrt{3(1 + 4B^2x^2)},$$

is determined by parameter $B = 12\gamma + 1$, which is also defined by Eq. (17). Thus, from the full set of three constants α , γ , and δ in Eq. (2), two parameters, α and δ , control the motion of the RW peak in solution (18), while the third parameter, γ , determines the temporal distance between the two depressions.

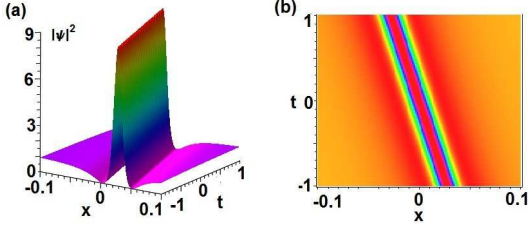


FIG. 5. (a) The evolution of the W-shaped profile and (b) 2D density contour plot for rational soliton (25) with $\alpha = 1$, $\gamma = -1/12$ and $\delta = 1$.

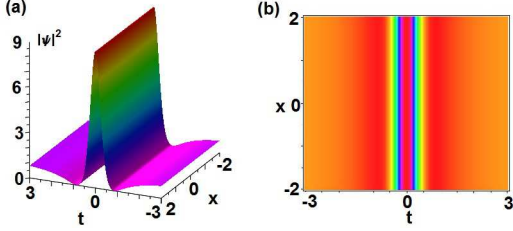


FIG. 6. (a) The evolution of the W-shaped intensity profile and (b) 2D intensity contour plot for rational soliton (25) at $\alpha = -5$, $\gamma = -1/12$ and $\delta = 1$.

To illustrate the structure and dynamical properties of the first-order RW solution (18) at different parameters, we choose sets $(\alpha = 1, \gamma = 1, \delta = 1)$ and $(\alpha = 5, \gamma = 3, \delta = 1)$ to display traces of peak (23) and depressions (24) in Figs. 1(a) and 2(a). Further, the evolution of the absolute value of the field at the peak and depression points is shown in Figs. 1(b,c) and 2(b,c).

Lastly, 2D density contour plots of the RW solution (18) are presented in Figs. 3 and 4 for different parameters.

2. The first-order rational soliton with $\gamma = -1/12$

For the case of $\gamma = -1/12$, we find that rational solution (18) becomes a solitary-wave solution of Eq. (2),

$$\psi_{1\gamma}(x, t) = \left[1 - \frac{4}{1 + 4(t + vx)^2} \right] e^{ix/2}, \quad (25)$$

which is a rational soliton-like solution of (2) with properties

$$|\psi_{1\gamma}(x, t)|^2 \rightarrow 1 \quad \text{as } |t + vx| \rightarrow \infty,$$

$$|\psi_{1\gamma}(x, t)|^2 \rightarrow 9 \quad \text{as } t + vx \rightarrow 0,$$

$$\max(|\psi_{1\gamma}(x, t)|^2) = 9 \quad \text{as } t + vx = 0,$$

$$\min(|\psi_{1\gamma}(x, t)|^2) = 0 \quad \text{as } |t + vx| = \sqrt{3}/2,$$

Rational soliton (25) feature W-shaped profiles at all x , as shown in Figs. 5 and 6.

Next, we analyze critical points of the intensity of the rational solution (25). It follows from Eq. (25) that there are three critical points of $|\psi_{1\gamma}|^2$,

$$(\tilde{x}_1, \tilde{t}_1) = (x, -vx), \quad (\tilde{x}_{2,3}, \tilde{t}_{2,3}) = \left(x, -vx \pm \frac{\sqrt{3}}{2} \right), \quad (26)$$

whose trajectories are straight lines. It also follows from Eq. (25) that

$$\left(\frac{\partial^2 (|\psi_{1\gamma}(x, t)|^2)}{\partial x \partial t} \right)^2 - \frac{\partial^2 (|\psi_{1\gamma}(x, t)|^2)}{\partial t^2} \frac{\partial^2 (|\psi_{1\gamma}(x, t)|^2)}{\partial x^2} = 0,$$

at three critical points (26) [in agreement with Eqs. (21) and (22)], hence the points cannot be characterized on the basis of this equation.

On the other hand, the critical point $(\tilde{x}_1, \tilde{t}_1)$ is a maximum (peak), as

$$\frac{\partial^2 (|\psi_{1\gamma}(x, t)|^2)}{\partial t^2} = -192 < 0$$

at this point (see Figs. 5 and 6). Similarly, two critical points $(\tilde{x}_{2,3}, \tilde{t}_{2,3})$ are minima (depressions), as

$$\frac{\partial^2 (|\psi_{1\gamma}(x, t)|^2)}{\partial t^2} = 6 > 0$$

at these points (see Figs. 5 and 6).

B. Second-order rational solutions and trajectories of extreme points

To produce second-order RW solution of Eq. (2), we choose the first-order rational solution (18) found above as a new seed. Substituting it into the linear spectral problem based on Eqs. (3)-(7) with $\lambda = i$, we solve it to generate new complex functions $r_2(x, t)$ and $s_2(x, t)$,

$$\begin{aligned} r_2(x, t) &= [r_{21}(x, t) + ir_{22}(x, t)] e^{-i(B+1)x/4}, \\ s_2(x, t) &= [s_{21}(x, t) + is_{22}(x, t)] e^{i(B+1)x/4}, \end{aligned} \quad (27)$$

where $r_{2j}(x, t)$ and $s_{2j}(x, t)$ ($j = 1, 2$) are given by

$$\begin{aligned} r_{21}(x, t) &= \frac{c_1 \xi(x, t) + c_2 B \eta(x, t)}{4D_1(x, t)}, \\ r_{22}(x, t) &= \frac{-4c_2 B \xi(x, t) + c_1 \eta(x, t)}{8D_1(x, t)}, \\ s_{21}(x, t) &= \frac{4c_2 B \xi(-x, -t) - c_1 \eta(-x, -t)}{8D_1(x, t)}, \\ s_{22}(x, t) &= \frac{c_1 \xi(-x, -t) + c_2 B \eta(-x, -t)}{4D_1(x, t)}, \end{aligned} \quad (28)$$

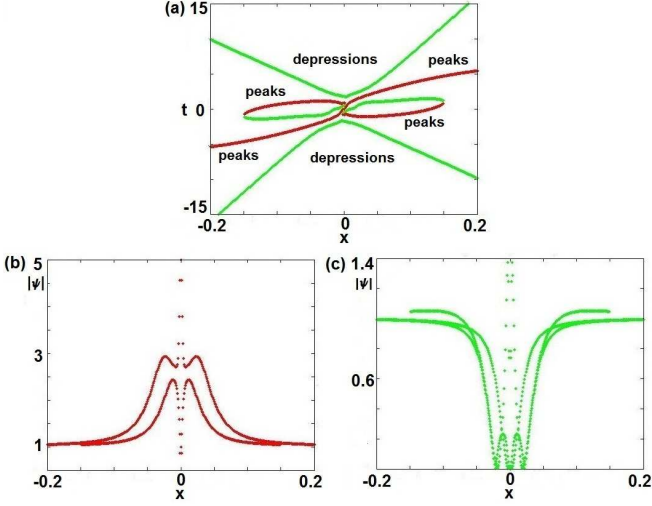


FIG. 7. (color online). The second-order rogue wave solution (30) for $\alpha = 2$, $\gamma = 3$ and $\delta = -1$. (a): The motion of the peak and depressions (red and green lines, respectively). (b) and (c): The evolution of the absolute values corresponding, severally, to the peak and depressions.

$$\begin{aligned}
 \xi(x, t) &\equiv 16Bv(B^2 + v^2)x^4 + 16B(B^2 + 3v^2)x^3t \\
 &\quad - 16B^3x^3 + 48Bvx^2t^2 + 16Bxt^3 \\
 &\quad + 4(120B\delta - 3Bv + 4v)x^2 \\
 &\quad + (8 - 20B)x + 4(4 - 7B)xt, \\
 \eta(x, t) &\equiv 16t^3(1 - t - 4vx) + 48(B^2 + v^2)x^2t \\
 &\quad + 12t - 96v^2x^2t^2 + 32(30\delta + v)xt \\
 &\quad + 4(7v + 120\delta)x + 16(B^4 - v^4)x^4 \\
 &\quad + 16v(3B^2 + v^2)x^3 \\
 &\quad + 8(7B^2 + 120\delta + 4v^2 - 4B),
 \end{aligned} \tag{29}$$

with expressions B , v , $D_1(x, t)$ given by Eqs. (17) and (19).

Substituting expressions (28) and (29) into system (27) and using Darboux transform (8) yields exact second-order rational solutions of Eq. (2) as

$$\psi_2(x, t) = \left[1 + \frac{G_2(x, t) + iK_2(x, t)}{D_2(x, t)} \right] \exp\left(\frac{i}{2}(1 + B)x\right). \tag{30}$$

Cumbersome expressions for real functions $D_2(x, t)$, $G_2(x, t)$, and $K_2(x, t)$ are given in the Appendix B. Particularly, for cases (i) $\alpha = \delta = \gamma = 0$, (ii) $\delta = \gamma = 0$, and (iii) $\alpha = \gamma = 0$, solution (30) yields the second-order RW solutions of NLS, Hirota, and LPD equations, respectively.

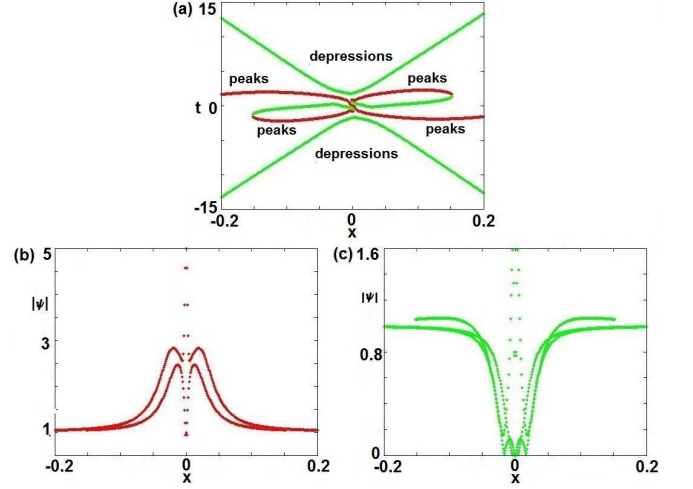


FIG. 8. (color online). The same as in Fig. 7, but for parameters $\alpha = -5$, $\gamma = 3$, and $\delta = 1$.

1. The second-order RW solution with $\gamma \neq -1/12$

To analyze dynamical properties of the second-order RW solution (30) with $\gamma \neq -1/12$, we first consider its intensity in the form of

$$|\psi_2(x, t)|^2 = \frac{[D_2(x, t) + G_2(x, t)]^2 + K_2^2(x, t)}{D_2^2(x, t)}. \tag{31}$$

Unlike the first-order rational solution (18), the peak and depressions of $|\psi_2(x, t)|^2$ cannot be obtained in an analytical form for expression (31) since we need to analytically solve two algebraic equations of the eleventh order for x and t , which are generated by $\{\partial(|\psi_2(x, t)|^2)/\partial x = 0, \partial(|\psi_2(x, t)|^2)/\partial t = 0\}$. Therefore, similar to what was done above for the first-order rational solution, we numerically analyze the respective trajectories with $\gamma \neq -1/12$ (e.g., $\gamma = 3$). The results are presented in Figs. 7 and 8, and the corresponding 2D contour plots are displayed in Figs. 9 and 10.

A characteristic difference of the second-order RW pattern from its first-order counterpart is that, in a limited interval of the evolution variable [namely, $|x| < 0.149$ and $|x| < 0.152$ in Figs. 7(a) and 8(a), respectively], in addition to the set of the single peak and two depressions, a new peak-depression pair appears.

To better represent the relevant solutions close to $x = 0$, trajectories of the peaks and depressions, and the evolution of the respective absolute values in the interval of $|x| \leq 0.01$ are displayed, for different parameters, in Figs. 11 and 12. In the case of $\alpha = 2$, $\gamma = 3$ and $\delta = -1$, there are two peaks and three depressions in the intervals of $-0.149 \leq x \leq -0.001$ and $0.001 \leq x \leq 0.149$, and there are three peaks and four depressions in the interval of $|x| \leq 0.001$. In the case of $\alpha = -5$, $\gamma = 3$ and $\delta = 1$,

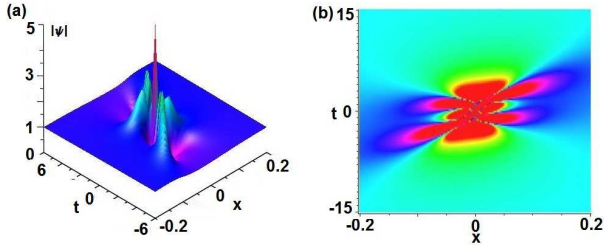


FIG. 9. (color online). The second-order rogue wave solution (30) at $\alpha = 2$, $\gamma = 3$, and $\delta = -1$. (a): The density evolution; (c) the corresponding 2D contour plot.

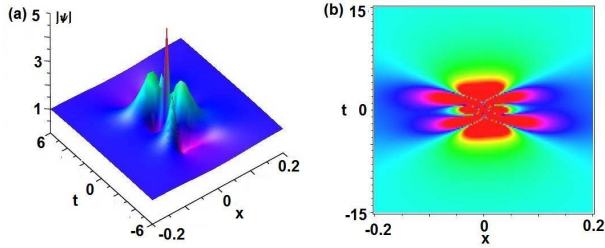


FIG. 10. (color online). The second-order rogue wave solution (30) at $\alpha = -5$, $\gamma = 3$, and $\delta = 1$. (a): The density evolution; (c) the corresponding 2D contour plot.

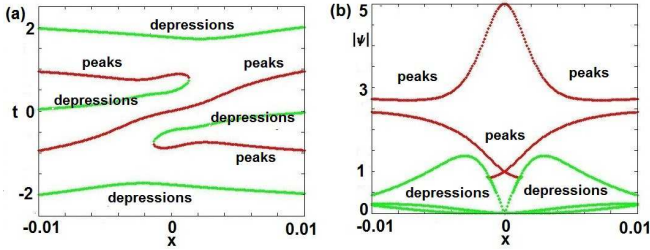


FIG. 11. (Color online). The second-order rogue wave solution (30) for $\alpha = 2$, $\gamma = 3$, and $\delta = -1$ in the vicinity of $x = 0$. (a): The motion of peaks and depressions (red and green lines, respectively). (b) The evolution of the absolute values of the peaks and depressions (red and green lines, respectively).

there are two peaks and three depressions in the intervals of $-0.152 \leq x \leq -0.001$ and $0.001 \leq x \leq 0.152$, and there are three peaks and four depressions at $|x| \leq 0.001$.

2. Rational soliton pair with $\gamma = -1/12$

For $\gamma = -1/12$, Eq. (30) yields rational two-soliton solutions of Eq. (2) as

$$\psi_{2\gamma}(x, t) = \left[1 + \frac{G_{2\gamma}(x, t) + iK_{2\gamma}(x, t)}{D_{2\gamma}(x, t)} \right] e^{ix/2}. \quad (32)$$

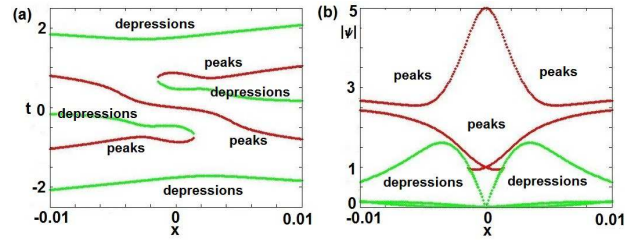


FIG. 12. (Color online). The second-order rogue wave solution (30) for $\alpha = -5$, $\gamma = 3$, and $\delta = 1$. (a): The motion of the peaks and depressions (red and green lines, respectively); (b) The evolution of the absolute values of the peaks and depressions (red and green lines, respectively).

Cumbersome expressions for real functions $D_{2\gamma}(x, t)$, $G_{2\gamma}(x, t)$, and $K_{2\gamma}(x, t)$ are given in the Appendix C.

Some profiles of two-soliton solutions (32) are displayed in Figs. 13 and 14 for $\alpha = 1$, $\delta = 1$ and $\alpha = -5$, $\delta = 1$, which display elastic interactions of two solitary waves. It follows from Fig. 14 that the amplitude of one solitary wave grows to a high limit value, and for the other solitary wave the amplitude falls to a low limit value at $|x| \rightarrow \infty$.

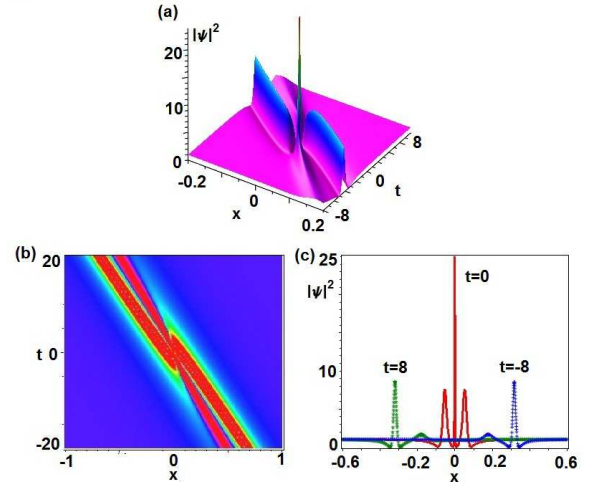


FIG. 13. (a) The interaction of two W-shaped solitons (32); (b) 2D density contour plots; and (c) cross sections for two-solitons (32), for $\alpha = \delta = 1$, and $\gamma = -1/12$.

V. CONCLUSIONS AND DISCUSSIONS

We have explicitly obtained the first- and second-order RW (rogue-wave) and rational-soliton solutions of the integrable fifth-order NLS equation belonging to the NLS hierarchy. It includes the fifth-order-dispersion and quintic-nonlinearity terms with three arbitrary real parameters [α , γ , and δ in Eq. (2)]. Several familiar in-

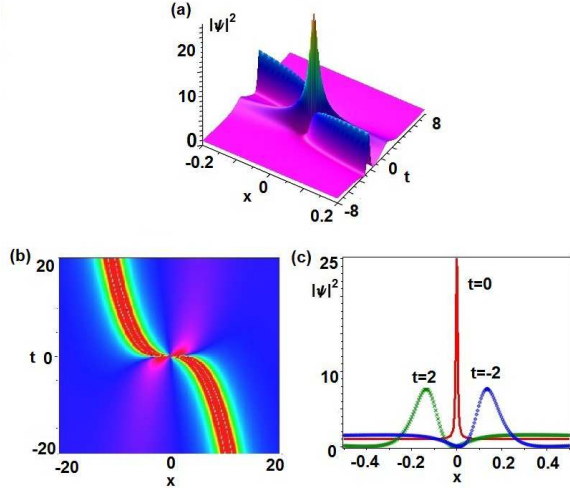


FIG. 14. (a) The interaction of two solitons (32); (b) 2D intensity contour plots; and (c) cross sections for two-solitons (32) for $\alpha = -5$, $\gamma = -1/12$, and $\delta = 1$.

tegrable models, such as the classical-NLS, Hirota, and LPD equations are particular cases of the FONLS equation, corresponding to particular values of α , γ , and δ , therefore, the previously studied RW solutions of those equations can be obtained as particular cases of our solutions (18) and (30).

The MI (modulation instability) of the flat CW background has been investigated in the framework of the FONLS equation, as it drives the formation of the RWs. The first-order RW exhibits one peak and two mutually symmetric depressions, while the second-order pattern generates an extra peak-depression pair, in a limited interval of the evolution variable. The location and motion of the peaks and depressions have been identified, in analytical and numerical forms. The structure and evolution of the RWs were elucidated by means of the density plots. Moreover, for the special case $\gamma = -1/12$, we obtain the corresponding one- and two-soliton solutions of Eq. (2), which are rational and W-shaped, being different from the usual bright and dark solitons.

We expect that the predicted results may be observed experimentally in various physical settings described by the general FONLS equation. It may be interesting to extend the analysis by further producing more complex patterns, such as those corresponding to third-order RWs and rational solitons, which will be studied in the future.

ACKNOWLEDGEMENTS

This work was supported by the National Natural Science Foundation of China (grants Nos. 61178091, 11326165, 11202178), and by the Zhejiang Provincial Natural Science Foundation of China under Grant No. LQ12A01008.

APPENDIX A

The explicit form of the system of equations $\{\partial(|\psi_1(x, t)|^2)/\partial t = 0, \partial(|\psi_1(x, t)|^2)/\partial x = 0\}$:

$$\begin{aligned}
& (t + 6x\alpha + 30x\delta)(3 - 4t^2 - 48tx\alpha - 240tx\delta - 144x^2\alpha^2 - 1440x^2\alpha\delta - 3600x^2\delta^2 \\
& + 1728x^2\gamma^2 + 288x^2\gamma + 12x^2) = 0, \\
& -64x + 276480t^2\alpha x\delta + 2488320t\alpha x^2\delta + 12441600t\alpha x^2\delta^2 + 663552t\alpha x^2\gamma^2 \\
& + 110592t\alpha x^2\gamma + 3317760t\delta x^2\gamma^2 + 552960t\delta x^2\gamma - 256x^3 - 5308416x^3\gamma^4 \\
& - 1769472x^3\gamma^3 - 221184x^3\gamma^2 - 12288x^3\gamma - 1152t\alpha - 5760t\delta - 6912x\alpha^2 - 172800x\delta^2 \\
& + 1536t^3\alpha + 7680t^3\delta + 331776x^3\alpha^4 + 207360000x^3\delta^4 + 768xt^2 - 9216x\gamma^2 - 1536x\gamma \\
& - 69120x\alpha\delta + 4608t\alpha x^2 + 23040t\delta x^2 + 691200t^2\delta^2x + 18432x\gamma t^2 + 110592x\gamma^2t^2 \\
& + 49766400x^3\alpha^2\delta^2 + 165888t\alpha^3x^2 + 165888000x^3\alpha\delta^3 + 20736000t\delta^3x^2 \\
& + 27648t^2\alpha^2x + 6635520x^3\alpha^3\delta = 0.
\end{aligned}$$

APPENDIX B

Functions D_2 , G_2 , and K_2 , which are parts of analytical solution (30), are given by the following expressions:

$$\begin{aligned}
D_2(x, t) = & 64t^6 + 384vxt^5 + 192(B^2 + 5v^2)x^2t^4 + 48t^4 + 256v(3B^2 + 5v^2)x^3t^3 - 64(120\delta + v)xt^3 \\
& + 192(B^2 + 5v^2)(B^2 + v^2)x^4t^2 + 108t^2 + 9 + 4(307B^2 + 57600\delta^2 + 5280\delta v \\
& + 139v^2 - 272B + 64)x^2 + 96(8B - 11B^2 - 240\delta v - 5v^2)x^2t^2 + 384v(B^2 + v^2)^2x^5t \\
& + 24(240\delta + 17v)xt + 192(120B^2\delta - 7B^2v - 120\delta v^2 - 3v^3 + 8Bv)x^3t + 64(B^2 \\
& + v^2)^3x^6 + 16(43B^2 + 1440B^2\delta v - 18B^2v^2 - 480\delta v^3 - 13v^4 - 16B^3 + 48Bv^2)x^4,
\end{aligned}$$

$$\begin{aligned}
G_2(x, t) = & -192t^4 - 1152(B^2 + v^2)x^2t^2 - 768vxt^3 - 288t^2 - 768v(3B^2 + v^2)x^3t - 192(120\delta + 7v)xt \\
& - 192(5B^2 + v^2)(B^2 + v^2)x^4 - (17B^2 + 240\delta v + 11v^2 - 8B)x^2 + 36,
\end{aligned}$$

$$\begin{aligned}
K_2(x, t) = & -384xt^4 - 768B(B^2 + 3v^2)x^3t^2 + 192(7B - 4)xt^2 - 1536Bv(B^2 + v^2)x^4t - 1536Bvx^2t^3 \\
& - 384(120B\delta - 3Bv + 4v)x^2t - 192(5B^3 + 240B\delta v + Bv^2 - 4B^2 + 4v^2)x^3 \\
& - 384B(B^2 + v^2)^2x^5 + 24(23B - 8).
\end{aligned}$$

APPENDIX C

Functions $D_{2\gamma}(x, t)$, $G_{2\gamma}(x, t)$, and $K_{2\gamma}(x, t)$, which are parts of analytical solution (32), are given by the following expressions:

$$\begin{aligned}
D_{2\gamma}(x, t) = & 64t^6 + 384xvt^5 + 960v^2t^4x^2 + 48t^4 + 1280v^3t^3x^3 - (7680\delta + 64v)t^3x \\
& + 960v^4t^2x^4 - (23040\delta v + 480v^2)t^2x^2 + 108t^2 + 384v^5tx^5 \\
& - (23040\delta v^2 + 576v^3)tx^3 + (5760\delta + 408v)tx + 64v^6x^6 \\
& - (7680\delta v^3 + 208v^4)x^4 + (256 + 230400\delta^2 + 21120\delta v + 556v^2)x^2 + 9,
\end{aligned}$$

$$\begin{aligned}
G_{2\gamma}(x, t) = & 36 - 192t^4 - 768t^3vx - 1152v^2t^2x^2 - 288t^2 - 768v^3tx^3 - 23040tx\delta \\
& - 1344xvt - 192v^4x^4 - 23040x^2\delta v - 1056x^2v^2,
\end{aligned}$$

$$K_{2\gamma}(x, t) = -192x [4(t + vt)^2 + 1].$$

-
- [1] L. Draper, *Mar. Obs.* **35**, 193 (1965).
 - [2] C. Kharif, E. Pelinovsky, and A. Slunyaev, *Rogue Waves in the Ocean* (Springer, Heidelberg, 2009).
 - [3] D. H. Peregrine, *J. Austral. Math. Soc. Ser. B (Appl. Math.)* **25**, 16 (1983).
 - [4] Y. C. Ma, *Stud. Appl. Math.* **60**, 43 (1979).
 - [5] N. Akhmediev and V. I. Korneev, *Theor. Math. Phys.* **69**, 1089 (1986).
 - [6] G. P. Agrawal, *Nonlinear Fiber Optics* (Academic Press: San Diego, 1995).
 - [7] B. A. Malomed, D. Mihalache, F. Wise, and L. Torner, *J. Opt. B Quantum Semiclassical Opt.* **7**, R53 (2005).
 - [8] Z. Y. Yan, *Phys. Lett. A* **374**, 672 (2010).
 - [9] C. Garrett and J. Gemmrich, *Phys. Today* **62**, 62 (2009).
 - [10] Z. Y. Yan, V. V. Konotop, and N. Akhmediev, *Phys. Rev. E* **82**, 036610 (2010).
 - [11] D. R. Solli, C. Ropers, P. Koonath, and B. Jalali, *Nature* **450**, 1054 (2007).
 - [12] Yu. V. Bludov, V. V. Konotop, and N. Akhmediev, *Phys. Rev. A* **80**, 033610 (2009).
 - [13] Z. Chen, M. Segev, D. N. Christodoulides, *Rep. Prog. Phys.* **75**, 086401 (2012).
 - [14] Z. Y. Yan, *Commun. Theor. Phys.* **54**, 947 (2010); Z. Y. Yan, *Phys. Lett. A* **375**, 4274 (2011).
 - [15] N. Akhmediev, J. M. Dudley, D. R. Solli, and S. K. Turitsyn, *J. Opt.* **15**, 060201 (2013).
 - [16] N. Akhmediev, A. Ankiewicz, M. Taki, *Phys. Lett. A* **373**, 675 (2009).

- [17] N. Akhmediev and E. Pelinovsky, Eur. Phys. J. Special Topics **185**, 1 (2010).
- [18] Z. Y. Yan, J. Phys.: Conf. Ser. **400**, 012084 (2012).
- [19] H. Hennig, Physics. **7**, 31 (2014).
- [20] T. B. Benjamin and J. E. Feir, J. Fluid Mech. **27**, 417 (1967).
- [21] P. A. E. M. Janssen, J. Phys. Oceanography **33**, 863 (2003).
- [22] K. Dysthe, H. E. Krogstad, and P. Müller, Ann. Rev. Fluid Mech. **40**, 287 (2008).
- [23] A. I. Dyachenko and V. E. Zakharov, JETP Lett. **81**, 255 (2005).
- [24] D. R. Solli, G. Herink, B. Jalali, and C. Ropers, Nature Photon. **6**, 463 (2012).
- [25] A. Ankiewicz, J. M. Soto-Crespo, and N. Akhmediev, Phys. Rev. E **81**, 046602 (2010).
- [26] U. Bandelow and N. Akhmediev, Phys. Lett. A **376**, 1558 (2012).
- [27] S. Chen, Phys. Rev. E **88**, 023202 (2013).
- [28] S. Xu and J. He, J. Math. Phys. **53**, 063507 (2012).
- [29] L. Wang, K. Porsezian, and J. He, Phys. Rev. E **87**, 053202 (2013).
- [30] A. Chowdury, D. J. Kedziora, A. Ankiewicz, and N. Akhmediev, Phys. Rev. E **91**, 022919 (2015).
- [31] X. Y. Wen, Y. Q. Yang, and Z. Y. Yan Phys. Rev. E **92**, 012917 (2015).
- [32] Y. Ohta and J. K. Yang, Phys. Rev. E **86**, 036604 (2012).
- [33] H. N. Chan, K. W. Chow, D. J. Kedziora, R. H. J. Grimshaw, and E. Ding, Phys. Rev. E **89**, 032914 (2014).
- [34] K. B. Dysthe and K. Trulsen, Phys. Scr. **T82**, 48 (1999).
- [35] F. Baronio, A. Degasperis, M. Conforti, and S. Wabnitz, Phys. Rev. Lett. **109**, 044102 (2012).
- [36] B. Guo and L. Ling, Chin. Phys. Lett. **28**, 110202 (2011).
- [37] F. Baronio, M. Conforti, A. Degasperis, and S. Lombardo, Phys. Rev. Lett. **111**, 114101 (2013).
- [38] Z. Y. Yan, Nonlinear Dyn. **79**, 2515 (2015).
- [39] Z. Y. Yan and C. Q. Dai, J. Opt. **15**, 064012 (2013).
- [40] Y. Q. Yang, X. Wang, and Z. Y. Yan, Nonlinear Dyn. **81**, 833 (2015).
- [41] A. Chowdury, D. J. Kedziora, A. Ankiewicz, and N. Akhmediev, Phys. Rev. E **90**, 032922 (2014).
- [42] T. Kano, J. Phys. Soc. Jpn. **58**, 4322 (1989).
- [43] R. Hirota, J. Math. Phys. **14**, 805 (1973).
- [44] M. Lakshmanan, K. Porsezian, and M. Daniel, Phys. Lett. A **133**, 483 (1988).
- [45] N. Akhmediev and N. V. Mitskevich, IEEE J. Quantum Electron. **27**, 849 (1991).
- [46] N. Akhmediev, J. M. Soto-Crespo, and A. Ankiewicz, Phys. Lett. A **373**, 2137 (2009).
- [47] L. Ling and L. Zhao, Phys. Rev. E **88** 043201 (2013).
- [48] V. B. Matveev and M. A. Salle, *Darboux Transformation and Solitons* (Springer-Verlag, Berlin, 1991).